processes

MDPI

Article

Enhanced Cadmium Adsorption Mechanisms Utilizing Biochar Derived from Different Parts of Wetland Emergent Plants *Iris sibirica* L.

Tongtong Li [1], Yangyang Wang [2,3], Yongchao Niu [4], Zhonglei Zhang [5], Jin Liu [2,3], Xiaoshu Wang [2], Jingao Wang [6], Ji Li [2,*] and Lei Wang [2,3,*]

1 Technical Centre for Soil, Agriculture and Rural Ecology and Environment, Ministry of Ecology and Environment, Beijing 100012, China
2 School of Materials & Environmental Engineering, Shenzhen Polytechnic University, Shenzhen 518055, China; xshuwang@163.com (X.W.)
3 Eco-Environmental Science Center (Guangdong, Hong-Kong, Macau), Ministry of Ecology and Environment, Guangzhou 510555, China
4 Bceg Environmental Remediation Co., Ltd., Beijing 100015, China
5 China North Energy Conservation and Environment Protection Co., Ltd., Beijing 100070, China
6 School of Chemical and Environmental Engineering, China University of Mining and Technology-Beijing, Beijing 100083, China; wangja0112@163.com
* Correspondence: liji@mail.szpt.edu.cn (J.L.); wangleicraes@163.com (L.W.)

Abstract: Due to their substantial biomass and rapid growth, emergent plants found in wetlands are viewed as excellent sources for biochar production, which has been demonstrated to serve as an effective substitute for absorbite in the effluent treatment. This article systematically contrasted the physicochemical properties of biochar derived from each section of *Iris sibirica* L. (designated as BC_R, BC_S, and BC_L) under identical pyrolysis conditions, in order to assess their effectiveness in removing cadmium (Cd) from effluent. Experimental results indicated that the removal efficiencies of Cd among the various biochars followed the order BC_S (19.92 mg/g) > BC_L (19.89 mg/g) > BC_R (13.22 mg/g). The removal of Cd^{2+} by biochar is primarily governed by chemisorption, as described by the Langmuir and Freundlich models. Moreover, different adsorption kinetic models, e.g., first-order kinetics, second-order kinetics, intra-particle diffusion, and the Elovich model, were performed to elucidate the adsorption process. Compared to BC_L and BC_R, the proportions of ion exchange and precipitation were more superior in BC_S, reaching 54% and 31%, respectively, which could serve as an effective adsorbent for metal ions, achieving the maximum adsorption capacity. In addition, precipitation (46%) was predominant during the Cd^{2+} adsorption process through BC_R. Therefore, BC_R was more suitable for the acidic wastewater treatment. This study provided an in-depth understanding of the cadmium removal behavior through biochar obtained from different part (roots, stems, and leaves) of wetland plants and introduced a new option for efficient utilization of waste biomass.

Keywords: wetland emergent plants; biochar; cadmium; adsorption; mechanism

check for updates

Academic Editor: Vijaya Raghavan

Received: 25 March 2025
Revised: 6 May 2025
Accepted: 13 May 2025
Published: 15 May 2025

Citation: Li, T.; Wang, Y.; Niu, Y.; Zhang, Z.; Liu, J.; Wang, X.; Wang, J.; Li, J.; Wang, L. Enhanced Cadmium Adsorption Mechanisms Utilizing Biochar Derived from Different Parts of Wetland Emergent Plants *Iris sibirica* L. *Processes* **2025**, *13*, 1520. https://doi.org/10.3390/pr13051520

Copyright: © 2025 by the authors. Licensee MDPI, Basel, Switzerland. This article is an open access article distributed under the terms and conditions of the Creative Commons Attribution (CC BY) license (https://creativecommons.org/licenses/by/4.0/).

1. Introduction

Metallic element pollution is a huge challenge for public health and ecosystems [1]. Especially, as one of the key hazardous harmful metals [2], cadmium (Cd) has been widely used in modern industrial and agricultural applications, such as electroplating, combustion of fossil fuels, wastewater irrigation, and abuse of agrochemicals [3]. The exposure of Cd^{2+} reduces plant growth by inhibiting chlorophyll biosynthesis and photosynthesis [4], and

causes severe risk to public health through the food web [5,6]. Among the widespread technologies developed to remove Cd^{2+} from wastewater [7], adsorption is a most promising technology with the advantages of being efficient, maneuverable, and low cost [8]. However, adsorption still faces challenges in seeking reasonable adsorbents for promoting the Cd^{2+} removal efficiency [9,10].

Generally, biochar is derived from biomass under limited oxygen or anaerobic conditions (N_2, Ar, or CO_2 atmosphere) between around 300 °C and 1000 °C [11–14]. Considering its excellent ion exchange characteristics, pore structure, and extensive surface functional groups, extensive research has been carried out on biochar for the removal of Cd^{2+} [15,16]. Emergent wetland species, including *Cyperus papyrus* (4.30 kg/m^2 dry biomass) and *Phragmites australis* (3.74 kg/m^2 dry biomass), exhibit fast-growing traits and significant biomass yields during reproductive stages, rendering them effective raw materials for biochar synthesis. Cui et al. investigated the adsorption of Cd^{2+} using biochar derived from various wetland plants, and the Cd^{2+} accumulation demonstrated clear variations across the various organs of plants [17]. Thus, it is essential to take into account the adsorption properties of biochar obtained from each section of wetland vegetation. As reported, the thermal decomposition temperature significantly impacts the physical and chemical characteristics of biochar, including the surface complexation, ion exchange, and Cd^{2+}–π interaction. As the pyrolysis temperature increases, the amount of carbon grows, whereas the hydrogen and oxygen levels diminish, leading to a greater presence of aromatic structures and a reduction in surface functional groups within the biochar. The study of Luo exhibited that the Ca^{2+} concentration significantly suppressed the Cd^{2+} adsorption capacity of biochar instead of K^+. These phenomena might be attribute to electrostatic repulsion, competitive effects, etc. In addition, the potential mechanisms for Cd^{2+} adsorption were proposed: (i) Cd^{2+} forms precipitates with anions (e.g., CO_3^{2-} and PO_4^{3-}) [18], (ii) the replacement of metal ions with Cd^{2+} (e.g., K^+, Ca^{2+}, and Na^+) [19], (iii) the interaction of Cd^{2+} with oxygen-containing functional groups through surface complexation [20], and (iv) Cd^{2+} coordination toward π electrons [21]. Consequently, the removal of Cd^{2+} by biochar is also associated with its alkalinity and the oxygen-containing functional groups, including aromatic, carboxylic, and hydroxy functional groups. These four factors occurred simultaneously during the Cd^{2+} adsorption process. Surface complexation was related to the stable inner complexation chemisorption and unstable outer complexation physical adsorption of biochar, while the strength of complexation was related to the charge number and hydration degree of metal ions. The electronegativity of biochar was also considered as the source of electrostatic action, enabling it to attract metal ions effectively through strong electrostatic forces. The adsorption mechanism was partially influenced by hydrolysis-driven metal precipitation triggered by the alkaline properties inherent in biochar materials.

Herein, we obtain the biochar from the root, stem, and leaf of *Iris sibirica* L., denoted as BC_R, BC_S, and BC_L, to explore the removal effect of Cd^{2+}. The material has a complex pore structure and combines a variety of surface functional groups, including carboxyl and phenolic hydroxyl groups. In addition, the adsorption effect and underlying mechanism of as-prepared biochar are studied in detail. More importantly, the adsorption characteristics of the synthesized biochar material are comprehensively investigated to elucidate the underlying removal mechanisms. With its extremely low cost-efficiency, easy operation, and high removal effect, the biochars derived from *Iris sibirica* L. are expected to achieve win–win results for carbon sequestration and water pollution.

2. Materials and Methods

2.1. Feedstock Collection and Biochar Preparation

Iris sibirica L., six months old and exhibiting similar visual traits in biomass, was meticulously transplanted from a nursery located in the Daxing district of Beijing. Initially, the plants underwent thorough washing with running tap water to eliminate any residual sediment, followed by rinsing with deionized water. Next, each plant was dissected into roots (including rhizomes and roots), stems, and leaves and oven-dried at 70 °C for 72 h. Then, the obtained biomass was crushed into powder and passed through a 100-mesh sieve. Next, 5.00 g of biomass powder was pyrolyzed in a tube furnace at 900 °C for 120 min under argon (Ar) gas conditions (ca. 200.00 mL/min) and then annealed to room temperature within 200 min. Biochars produced from roots, stems, and leaves of *Iris sibirica* L. were labeled as BC_R, BC_S, and BC_L, respectively. Finally, obtained biochars were hand-grounded into powders and sieved through 100 mesh.

2.2. Experiments

A sequence of adsorption tests was conducted to evaluate the biochars' capacity for removing Cd^{2+}. These tests were performed in 50.0 mL centrifugal tubes using a horizontal vibrator (HZX-Q100, China) at 200 rpm. To prepare specific concentrations of Cd^{2+}, dilutions were made from a standard stock solution (500.00 mg/L) derived from $Cd(NO_3)_2{\cdot}4H_2O$, using a $NaNO_3$ solution (0–1.00 mol/L) as the background electrolyte. The supernatant was leached by a 0.22 μm membrane. A series of kinetic experiments was performed with 0.02 g of biochar in 20.00 mL of Cd^{2+} solution (initial concentration: 20.0 mg/L) for contact times from 0 to 1440 min. In addition, 0.01 mol/L of $NaNO_3$ was selected as the electrolyte. The system was maintained at 25 °C, pH 5.5. The adsorption equilibrium parameters were obtained through systematic variation of Cd^{2+} solution concentrations (0–500 mg/L) under controlled temperature conditions (15–45 °C), utilizing a fixed sorbent dosage of 1.00 g/L with 24 h of equilibration to establish isothermal profiles. Besides, Cd^{2+}, K^+, Ca^{2+}, and Mg^{2+} were analyzed using an inductively coupled plasma–mass spectrophotometer (ICP-MS) instrument (Agilent 7500cx, USA). All chemicals used in this research were analytical-grade reagents (SCRC, Sinopharm Chemical Reagent Co., Ltd., China).

The removal efficiency (*RE*, %) and adsorptive efficiency (Q_t, mg/g) were measured from the following equations [22]:

$$RE = \frac{c_0 - c_e}{c_0} \times 100\% \quad (1)$$

$$Q_t = \frac{(c_0 - c_t) \times V}{m} \quad (2)$$

$$Q_e = \frac{(c_0 - c_e) \times V}{m} \quad (3)$$

where Q_t (mg/g) is the adsorption amount of Cd^{2+} at any instant t, Q_e (mg/g) is the adsorption amount of Cd^{2+} at the balanced moment, c_0 (mg/L), c_e (mg/L), and c_t (mg/L) are the initial, balanced, and any instant t of Cd^{2+} concentration, respectively, V (L) is the solution volume, and m (g) is the amount of used biochar.

2.3. Kinetics Analysis

The following equations are different adsorption kinetic models:

$$\text{First-order kinetic equation}: \ Q_t = Q_e\left(1 - e^{-k_1 t}\right) \quad (4)$$

$$\text{Second-order kinetic equation}: \ Q_t = \frac{Q_e{}^2 k_2 t}{1 + k_2 Q_e t} \tag{5}$$

$$\text{Intra-particle diffusion equation}: \ Q_t = k_p t^{0.5} + c \tag{6}$$

$$\text{Elovich equation}: \ Q_t = \frac{1}{\beta} \ln t + \frac{1}{\beta} \ln(\alpha\beta) \tag{7}$$

where Q_e represents the equilibrium adsorption capacity of biochar (mg/g), Q_t denotes the adsorption capacity of biochar at time t (mg/g), and k_1 refers to the adsorption rate constant associated with Equation (4) (min^{-1}). In addition, k_2 indicates the adsorption rate constant related to Equation (5) (g/(mg·min)), while k_p is the reaction rate constant for Equation (6). Further, α represents the initial adsorption rate of Equation (7) (mg/(g·min)), and β is the Elovich analytical constant, which is linked with both chemical adsorption activation energy and surface coverage (g/mg).

2.4. Isothermal Equilibrium Analysis

To investigate the effects of temperatures and initial Cd^{2+} concentrations, the Langmuir model was used:

$$\text{Langmuir model}: \ Q_e = \frac{k_l Q_m c_e}{1 + k_l c_e} \tag{8}$$

$$\text{Freundlich model}: \ Q_e = k_f c_e^{1/n} \tag{9}$$

where c_e represents the equilibrium adsorption concentration (mg/L), Q_e and Q_m denote the equilibrium adsorption capacity and its maximum value (mg/g), respectively, while k_l refers to the parameters of the Langmuir model (L/mg), and k_f and n correspond to the Freundlich parameters associated with the capacity for reaction adsorption and the strength of adsorption, respectively.

2.5. Contribution of Cd^{2+} Adsorption

To analyze the different underlying mechanisms of Cd^{2+} adsorption on biochar, four experiments were performed: (I) biochar, (II) biochar washed by high-purity water until the pH was stable, (III) biochar adjusted with stable pH, and (IV) biochar with stable pH and further adjusting the initial pH. A series of kinetic experiments was performed with 0.02 g of biochar in 20.00 mL of Cd^{2+} solution (initial concentration: 20.0 mg/L) for contact times from 0 to 1440 min. Metal ion exchange (Q_{cme}), mineral precipitation (Q_{cmp}), and other adsorption effects (Q_{other}) were precisely analyzed [17,23].

The mineral-associated adsorption component (designated as Q_{cm}) was quantitatively evaluated through the following mathematical formulation:

$$Q_{cm} = Q_t - Q_a Y \tag{10}$$

where the variable Q_{cm} (mg/g) represents the Cd^{2+} adsorption amount for the interactions with minerals, while Q_t (mg/g) indicates the adsorption of Cd^{2+} on biochar (group II). Additionally, Q_a (mg/g) refers to the quantity of Cd^{2+} that has been sorbed on biochar following acid washing with 0.10 M HCl (group III). Lastly, Y denotes the ratio of the demineralized biochar and the fresh biochar. The quantities of K^+, Ca^{2+}, and Mg^{2+} from biochars into the solution were evaluated and illustrated in the figure both prior to and following the adsorption process. Consequently, the Cd^{2+} adsorption attributed to ion exchange (Q_{cme}) was expressed by Equation (11):

$$Q_{cme} = Q_K + Q_{Ca} + Q_{Mg} \tag{11}$$

where Q_K, Q_{Ca}, and Q_{Mg} are the metal amounts released from biochar after the adsorption process (group III).

Cd^{2+} adsorption (Q_{cmp}) caused by precipitation was measured by the difference value of Q_{cm} and Q_{cme}:

$$Q_{cmp} = Q_{cm} - Q_{cme} \quad (12)$$

Other adsorption effects (Q_{other}) could be obtained by removing these effects from the total adsorption capacity:

$$Q_{other} = Q_t - Q_{cme} - Q_{cmp} \quad (13)$$

2.6. Characterization of Biochar

The Brunauer–Emmett–Teller (BET) N_2 adsorption technique was measured utilizing the Tristar 3020 M instrument (USA). To capture the surface morphology, images were acquired using a scanning electron microscope (SEM; SU8010, Hitachi, Japan). X-ray diffraction (XRD) patterns of the biochars were analyzed using an X-ray diffractometer (Bruker-AXS, Karlsruhe, Germany). Additionally, the functional groups and chemical bonding were recognized with a Fourier transform infrared spectrometer (FTIR, Bruker VERTEX 70, Germany), covering a spectral range from 4000 to 500 cm^{-1}.

2.7. The Yield, pH, Zeta Potential, and Ash Content of Biochar

The yield of biochar at different pyrolysis temperatures was calculated according to the following formula [24,25]:

$$y = \frac{m_2}{m_1} \times 100\% \quad (14)$$

where y represents the yield of biochar (%), m_1 is the amount of biomass (g), and m_2 is the amount of biochar obtained after carbonization of biomass raw material (g).

The as-prepared biochar was put into pure water with a proportion of 1.00 g/L and shaken in a shaking box at 200 r/min for 2 h (at 25 °C). The biochar was separated from the filtrate and washed off by a suction filtration device. Each biochar sample was tested three times [24].

Zeta potential was measured using a Zetasizer nano (UK) at different pH values [24,26,27].

The determination of ash content was conducted according to the ASTM D1782-84 [28], where 1.00 g of biochar was put into muffle furnace at 750 °C for 6 h. The mass of the residue was weighed to calculate the ash content of the biochar [24,25]. Each biochar sample was determined in parallel three times.

3. Results and Discussions

3.1. Characterization of Biochars from Wetland Emergent Plants *Iris sibirica* L.

The yield, pH, and ash content of BC_R, BC_S, and BC_L obtained from *Iris sibirica* L. are shown in Table 1. Among the biomass raw materials, hemicellulose was the most easily pyrolyzed, followed by lignin, while cellulose pyrolysis was more complex, leading to some variability of the yielded data. Therein, the yield of BC_R was significantly higher than that of BC_S and BC_L, which might be determined by the most coke products provided by lignin [29].

Biochar obtained from *Iris sibirica* L. exhibited remarkable alkalinity, with a pH value exceeding 9. According to related research [30], the ash content in biochar could cause the biochar to be alkaline, and the high aromaticity in biochar was also responsible for the alkalinity of biochar. Biochar underwent anaerobic pyrolysis at elevated temperatures, leading to the formation of numerous voids in the material because of the release of volatile substance (e.g., cellulose or hemicellulose), which augmented the specific surface area

(SSA) of the biochar. Figure 1a–c show the N_2 adsorption–desorption isotherm curves and the pore size distribution curves of BC_R, BC_S, and BC_L. The structural composition of the biomass raw material led to differences in BET specific surface area, so the BC_R, BC_S, and BC_L were 120.36 m^2/g, 414.95 m^2/g, and 16.68 m^2/g, respectively, as shown in Table 1. The contaminant sequestration performance of the carbonaceous sorbents, as demonstrated through Langmuir-type adsorption modeling (Type I isotherm characteristics), exhibited strong linear correlations with SSA and mesoporous structural parameters. Due to the looser structure of BC_S, many volatile components inside would release under high temperatures, which was conducive to the production of pore structure, and then obtained the largest SSA. The total pore volumes of BC_R, BC_S, and BC_L were 0.07, 0.22, and 0.03 cm^3/g, respectively. Hence, the BC_S and BC_L with large total pore volumes were beneficial to Cd^{2+} adsorption on biochar. The micropore volumes of BC_R, BC_S, and BC_L were 0.04 cm^3/g, 0.15 cm^3/g, and 0.006 cm^3/g, respectively, so the BC_S and BC_L obtained better adsorption capacity.

Table 1. The basic characteristics of different biochars from *Iris sibirica* L.

Parameters	BC_R	BC_S	BC_L
Yield (%)	49.13%	28.06%	28.17%
pH	9.49	10.13	10.16
Ash content (%)	31.34%	26.83%	35.04%
BET ($m^2 \cdot g^{-1}$)	120.36	414.95	16.68
Micropore area ($m^2 \cdot g^{-1}$)	82.11	285.85	274.80
Total pore volume (P/P_0 = 0.992, $cm^3 \cdot g^{-1}$)	0.07	0.22	0.03
Micropore volume ($cm^3 \cdot g^{-1}$)	0.04	0.15	0.006
Average pore diameter (nm)	2.35	2.16	2.31

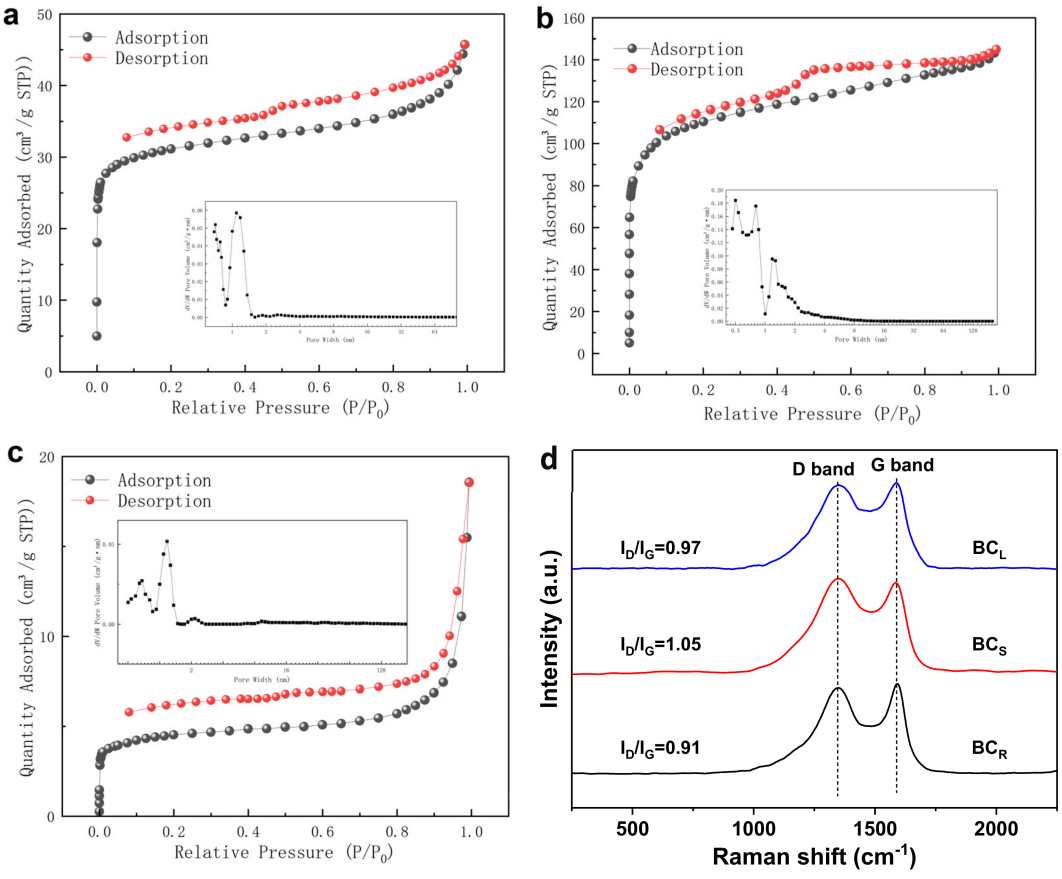

Figure 1. N_2 adsorption−desorption isotherm curves and the pore size distribution of BC_R (**a**), BC_S (**b**), and BC_L (**c**). (**d**) Raman spectra of the BC_R, BC_S, and BC_L.

The defect degree in biochars was quantitatively analyzed by the Raman spectra. As shown in Figure 1d, peaks at 1350 and 1590 cm^{-1} corresponding to D- and G-bands were recognized as the disordered sp^2-hybridized carbon in polycyclic aromatic hydrocarbons and ordered graphitic carbon, respectively. The ID/IG was a reliable index of structural defects in graphitized biochars. Notably, the ID/IG ratio of BC_S (1.05) was significantly higher than those of BC_R (0.91) and BC_L (0.97), demonstrating that BC_S possessed a richer defect structure. This enhanced defect degree was expected to contribute to a larger SSA, as structural imperfections typically create additional active sites and porosity.

Figure 2a shows the XRD patterns of BC_R, BC_S, and BC_L obtained from *Iris sibirica* L. During the process of biochar carbonization, the state of carbon in biochar began to change from amorphous to crystalline. The XRD characterization suggested that the main component of BC_S and BC_L was KCl (PDF#41-1476), but the main component of BC_R was SiO_2 (PDF#46-1045), by comparing the strongest diffraction peaks of the copper crystalline planes, which should be ascribed to the interactions among different elements in the biochar during the pyrolysis process. According to related studies, SiO_2 had a positive effect on Cd^{2+} adsorption, and the K^+ of BC_S and BC_L can also provide sites for biochar to adsorb Cd^{2+} through ion exchange [31].

Figure 2b shows the FTIR spectroscopy results, which could be used to characterize the group in the structure of the reaction product, thereby inferring the molecular structure of the substance [32–34]. The BC_R, BC_S, and BC_L were vibrated, ranging from 3751 to 3568 cm^{-1}, demonstrating the existence of O-H bonding stretching vibration. Peaks observed at 1703 and 1022 cm^{-1} primarily corresponded to the C=O and C-O-C band stretching, respectively. The BC_L was vibrated more strongly than BC_R and BC_S at 1631 cm^{-1}, which was ascribed to the aromatic ring C=C bond vibration. The BC_S and BC_L had the characteristic peaks of C=O bonding and C-O of phenolic hydroxyl at 1438 cm^{-1} and 1325 cm^{-1}, respectively. The vibrations at 622 and 1523 cm^{-1} were, respectively, identified as sulfate and carbonate [35,36]. The vibrations at 1385 and 1650 cm^{-1} were ascribed to the carboxyl and anhydrides, respectively [37,38]. Furthermore, the fluctuation of 812 cm^{-1} to 628 cm^{-1} was caused by Si-O-Si bonding. Therefore, the BC_S had a pore structure with a large SSA, as well as abundant surface functional groups, such as carboxyl, phenolic hydroxyl, and acid anhydrides, which was considered as a stable adsorption site for both heavy metals and organics in sewage [39]. We performed SEM characterization of biochar to characterize the surface morphology of BC_R, BC_S, and BC_L, as shown in Figure 2c–e. Compared with BC_R, the surfaces of the BC_S and BC_L were more uniform, with more pore structures. It could be observed that many pores were blocked in the BC_S, whereas the pore structure of the BC_L was ordered and abundant (Figure 2e). Ash particles attached to the carbon skeleton that makes up the pore structure of biochar, as shown by the brighter color in Figure 2c–e. The ash in biochar was mainly composed of alkali metal, alkaline earth metal carbonates, phosphates, oxides, etc., which were randomly distributed in the outer surface and inner pores of the biochar. At these locations, the probability of adsorption occurring due to ion exchange and chemisorption, as opposed to physical functions, was elevated. The metal elements present on the surface were assessed using EDS. The main components of BC_S (Figure 2g), BC_R (Figure 2f), and BC_L (Figure 2h) were carbon, oxygen, potassium, calcium, and magnesium. It was deduced that BC_S had a chemically pure surface, characterized by a relatively dense distribution of different elements and a notably high level of carbonization. The elevated presence of minerals or inorganic compounds could be connected to the role of BC_S as elemental transport organs, suggesting that improved adsorption might be possible via ion exchange.

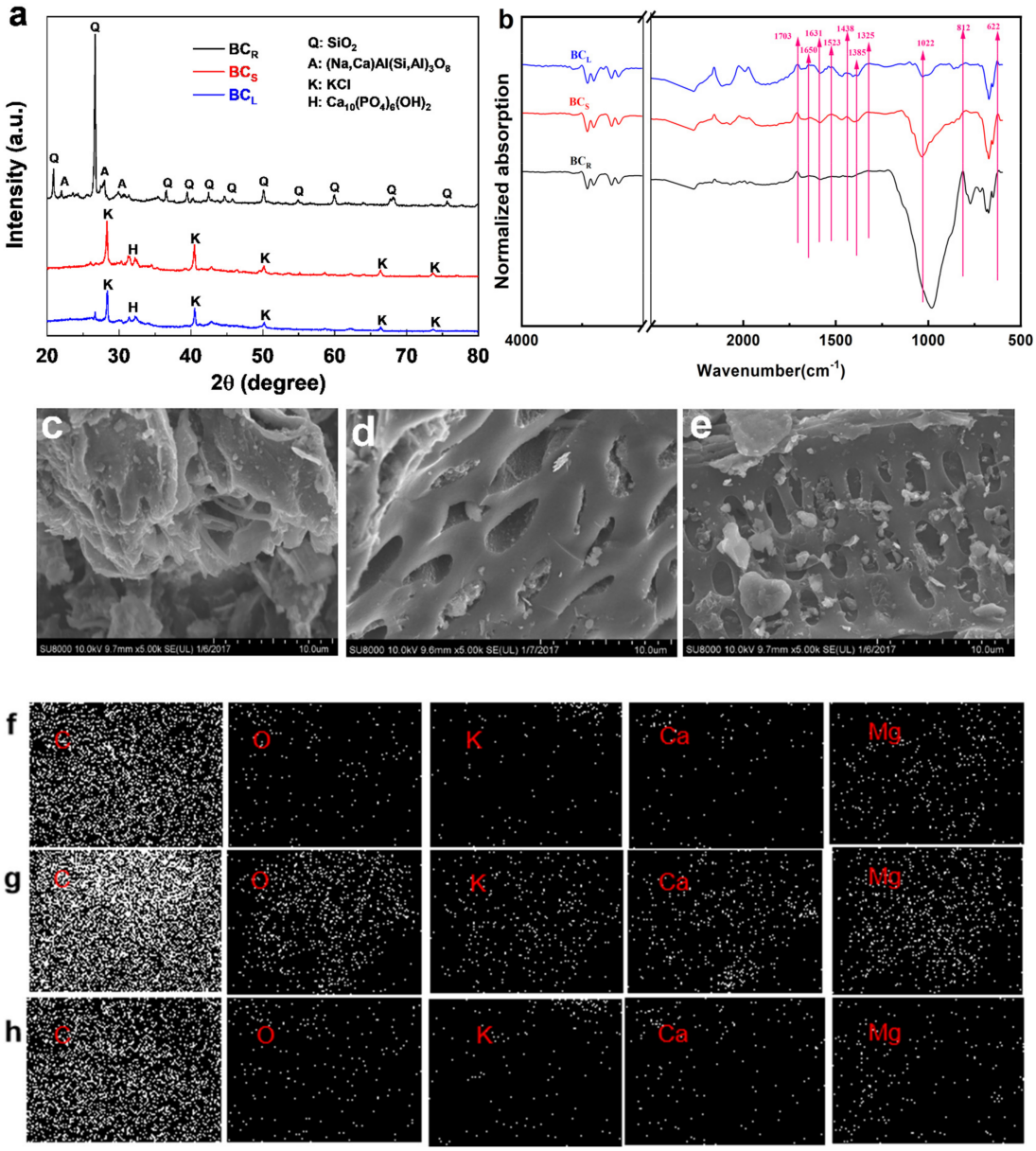

Figure 2. Characterization of biochar obtained from *Iris sibirica* L. (BC_R, BC_S, and BC_L). (**a**) XRD diffraction pattern, (**b**) FTIR, SEM images of (**c**) BC_R, (**d**) BC_S, and (**e**) BC_L, and EDS of (**f**) BC_R, (**g**) BC_S, and (**h**) BC_L.

3.2. Adsorption Fitting of Cd^{2+} by Biochars

3.2.1. Effect of Initial Heavy-Metal Concentration and Electrolyte Concentration on Adsorption

To explore the Cd^{2+} adsorption on biochar with different initial concentrations, the temperature and the amount of biochar were fixed at 298 K and 2 g/L, respectively. With the increasing of the initial Cd^{2+} contents, the adsorption efficiencies of BC_R, BC_S, and BC_L for Cd^{2+} gradually increased, as shown in Figure 3a. When the initial concentration of Cd^{2+} was not higher than 30.0 mg/L, the adsorption efficiencies of BC_S and BC_L were obviously greater in comparison with BC_R. The unsaturated surface sites had a strong affinity for Cd ions, thereby enhancing the adsorption performance of biochar in relatively low-concentration Cd solutions. This finding suggests that as the initial concentration rose, the concentration gradient at the interface between solid and liquid became steeper, facilitating the movement of Cd^{2+} from the solution to the adsorbent and subsequently enhancing the biochar's ability to adsorb Cd^{2+}.

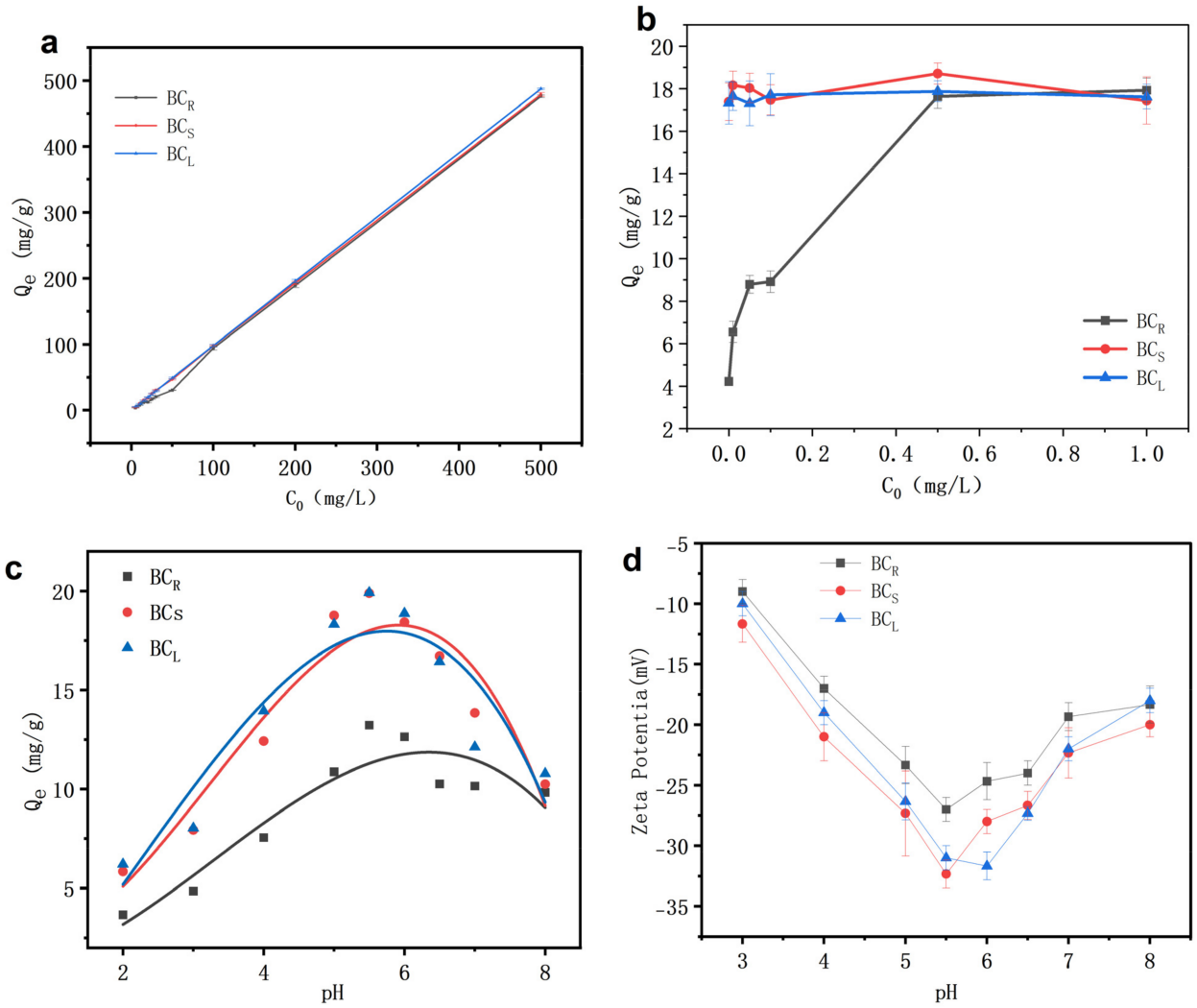

Figure 3. The dependent adsorption of (**a**) the initial concentration (initial Cd^{2+} concentration 5–500.00 mg/L, $NaNO_3$ concentration 0.01 mol/L, time 90 min, temperature 25 °C, volume 20.00 mL, dosage of biochar 0.02 g, and pH 5.5), (**b**) the electrolyte concentration of Cd^{2+} by BC_R, BC_S, and BC_L (initial Cd^{2+} concentration 20 mg/L, $NaNO_3$ concentration 0, 0.01, 0.05, 0.10, 0.50, and 1.00 mol/L, respectively, time 90 min, temperature 25 °C, volume 20.00 mL, dosage of biochar 0.02 g, and pH 5.5), (**c**) the pH change by BC_R, BC_S, and BC_L (initial Cd^{2+} concentration 20.00 mg/L, $NaNO_3$ concentration 0.01 mol/L, time 90 min, temperature 25 °C, volume 20 mL, dosage of biochar 0.02 g, and pH 2−8), and (**d**) the Zeta potential (ζ) of the BC_R, BC_S, and BC_L (pH 2–8).

The influence of ionic strength was examined and depicted in Figure 3b. The Cd^{2+} adsorption efficiency on BC_R was improved with the electrolyte content. As the $NaNO_3$ concentration approached 0.50 mg/L, the adsorption of Cd^{2+} appeared to stabilize. In contrast, the Cd^{2+} adsorption efficiencies on BC_S and BC_L changed little, and their adsorption efficiencies varied between 18.17 and 18.33 mg/g. When the $NaNO_3$ content exceeded 0.50 mg/L, the amount of adsorbed Cd was inversely proportional to the electrolyte content, indicating that Na^+ may occupy adsorption sites in BC_S and BC_L. The adsorption capacity of different electrolyte concentrations for cadmium could be divided into two styles [40]. The electrolyte content would intensify the competition of sites and thus depress the adsorption efficiency. The concentration of electrolytes could regulate the electrostatic effect, competing with the ion exchange, and form ion pairs with the adsorbate, which was considered as a factor that cannot be ignored for the adsorption process. The Cd^{2+} adsorption efficiency decreased with the increasing electrolyte content, from which it was inferred that the interaction of biochar with the soil surface could form

outer surface complexes. The significant chemical adsorption of metal ions can be ascribed to the inner-sphere surface complexation and cation exchange processes. However, once the adsorption efficiency increased or negligibly changed with the electrolyte strength, the inner surface complexes could be generated. Therefore, we could infer that Cd^{2+} reacted with surface functional groups to form inner surface complexes during the adsorption process by this variation [41]. The uptake of cadmium onto biochar diminished as the ionic strength rose within the lower pH spectrum. This increased electrolyte strength would significantly influence the electrostatic layer structure and the interfacial energy, leading to alterations in the intrinsic binding constants of the species that are adsorbed. To further uncover the effect of pH on Cd^{2+} removal efficiency by biochar, a systematic experimental investigation was conducted. As illustrated in Figure 3c, the adsorption Cd^{2+} efficiency on biochar increased significantly with a pH range of 2–6. Under acidic conditions (pH = 2), the H^+ competed with Cd^{2+} for limited sites, resulting in lower Cd^{2+} uptake, which was due to proton competition and cationic repulsion. Near-neutral pH (5–6) maximized uptake through deprotonated carboxyl/hydroxyl groups (-COO-/-O-), enabling electrostatic attraction and inner-sphere complexation with Cd^{2+}. The biochar derived from different organs (BC_R, BC_L, and BC_S) exhibited maximum equilibrium adsorption capacities at pH 5.5 (13.22, 19.89, and 19.92 mg/g, respectively), with corresponding removal efficiencies of 66.1%, 99.45%, and 99.60%. Compared with other carbon-based adsorbents, BC_L and BC_S demonstrated significantly enhanced adsorption performance for Cd^{2+}, thereby underscoring the potential advantages of *Iris sibirica* L.-derived biochar (Table S1) [25–27,42–44]. Nevertheless, a sluggish decline in adsorption performance was captured under pH 7–8. This phenomenon may be ascribed to (1) increased ionization of carboxyl groups, reducing available binding sites, and (2) the formation of Cd^{2+}-hydroxide complexes ($Cd(OH)^+$/$Cd(OH)_3^-$), which decreased the concentration of free Cd^{2+} ions and consequently diminished the adsorption capability of *Iris sibirica* L.

In Figure 3d, the Zeta potential of BC_S was inferior to that of BC_R and BC_L, which ranged from −10 mV to −33 mV with a pH range of 2–8. An elevation in pH led to a more negative Zeta potential, indicating a greater deprotonation of surface functional groups, including carboxyl and hydroxyl, as observed in the FTIR analysis [26]. Under conditions of low pH, the ability of carbonaceous materials to adsorb diminished because of the strong competition for binding to surface functional groups between hydrogen ions and Cd^{2+} cations. Moreover, the surplus of hydrogen ions resulted in the electrostatically repulsive force of Cd^{2+}. When the pH increased to 5.5–6, carboxyl and hydroxyl groups, along with other oxygen-containing functional groups, underwent deprotonation, thereby increasing negatively charged active sites, which enhanced the adsorption of Cd^{2+} via electrostatic attraction and surface complexation. Furthermore, as the solution pH rose, the decreasing concentration of H^+ minimized competition for active sites, allowing more Cd^{2+} cations to interact with the adsorbent and improving metal ion retention. However, when the pH exceeded 7, $Cd(OH)_2$ became predominant, reducing the free Cd^{2+}.

3.2.2. Study on the Kinetics of Cd^{2+} Adsorption by Biochar

The kinetic curves of adsorption were used to explore the change in the adsorption rate and heavy-metal diffusion on the adsorbent, which provided theoretical bases for the adsorption of heavy metals by biochar. At this point, different adsorption kinetic models, such as first-order kinetics, second-order kinetics, intra-particle diffusion, and the Elovich model, were applied to reveal the adsorption procedure. The fitting parameters are presented in Table 2. It was assumed in the first-order kinetic model that the adsorption rate was proportional to the number of un-adsorbed sites on the solid phase [45]. However, the adsorption processes of the BC_R, BC_S, and BC_L fit the second-order kinetics

better compared to first-order kinetics, especially the R^2 of BC_S, which was 0.66 and 0.96, respectively, as shown in Figure 4a,b. Therefore, the chemical mechanism of adsorption, including the interaction involving electron sharing and transfer, may influence the biochar's adsorption rate.

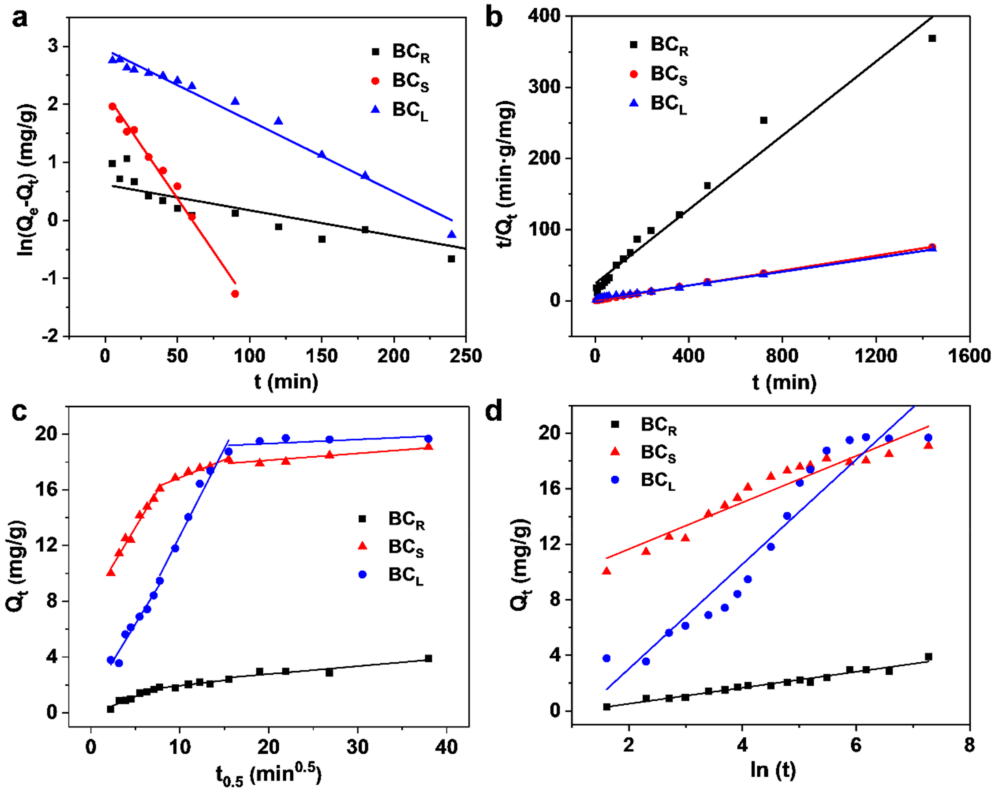

Figure 4. Model fitting of adsorption of Cd^{2+} by BC_R, BC_S, and BC_L of *Iris sibirica* L. (**a**) First−order kinetics, (**b**) second−order kinetics, (**c**) intra−particle diffusion model, and (**d**) Elovich model (time 5–1440 min, initial Cd^{2+} concentration 20.00 mg/L, $NaNO_3$ concentration 0.01 mol/L, temperature 25 °C, volume 20.00 mL, dosage of biochar 0.02 g, and pH 5.5).

The intra-particle diffusion model was frequently employed to examine the controlling steps in both the reaction and adsorption processes. These processes can be categorized into three stages: the adsorption of the adsorbent on the surface, gradual adsorption, and the attainment of equilibrium adsorption. The first stage was the Cd^{2+} diffusion through the liquid film to the outer surface, and the slope of the line reflected the magnitude of the reaction rate. The second stage of adsorption of Cd^{2+} by BC_R, BC_S, and BC_L could be fitted well by the intra-particle diffusion model ($R^2 > 0.83$), as shown in Figure 4c, indicating that the adsorption of Cd^{2+} by biochar was controlled by the intra-particle diffusion process. Numerous research works have indicated that the rate-limiting factor for the adsorption of heavy-metal ions by biochar is intra-particle diffusion. Wang et al. reported that the adsorption process of Cd^{2+} on Ni-doped bamboo charcoal could be divided into three stages: the membrane diffusion process, the interaction between Cd^{2+} and adsorption sites on the outer surface of bamboo charcoal, and the intra-particle diffusion process [23]. Besides, k_p (stage 1) > k_p (stage 2) implied that as Cd^{2+} gradually occupied adsorption sites on the surface of the material, increasing the thickness of the boundary layer reduced the internal diffusion rate. The reaction process of biochar treatment of Cd^{2+} had a multi-effect, as it fit the linearity of the first stage and did not go through the origin. Therefore, intra-particle diffusion was not the only rate-limiting process for the adsorption of Cd^{2+} by biochar, and the process of Cd^{2+} diffusion from solution through the membrane to the biochar surface was also the key.

Table 2. Fitting parameters of first-order kinetics, second-order kinetics, intra-particle diffusion, and the Elovich model of Cd^{2+} adsorption by BC_R, BC_S, and BC_L of *Iris sibirica* L.

	First-Order Kinetics			Second-Order Kinetics			Elovich			Intra-Particle								
										Stage 1			Stage 2			Stage 3		
	K_1 (min^{-1})	q_e (mg/g)	R^2	K_1 (min^{-1})	q_e (mg/g)	R^2	α (mg/g·min)	β (mg/g)	R^2	k_p (mg/(g·$min^{0.5}$))	c (mg/g)	R^2	k_p (mg/(g·$min^{0.5}$))	c (mg/g)	R^2	k_p (mg/(g·$min^{0.5}$))	c (mg/g)	R^2
BC_R	0.013	2.934	0.818	0.005	3.384	0.888	0.192	1.737	0.963	0.26	−0.14	0.95	0.075	1.196	0.83	0.056	1.655	0.83
BC_S	0.095	17.148	0.663	0.001	21.939	0.964	232.320	0.595	0.909	1.27	0.07	0.98	0.257	14.312	0.96	0.049	17.150	0.83
BC_L	0.012	19.533	0.962	0.009	18.154	0.913	1.139	0.265	0.914	1.049	1.123	0.96	1.255	0.137	0.97	0.029	18.757	0.39

In addition, we also performed Elovich model fitting for adsorption of Cd^{2+} by BC_R, BC_S, and BC_L, and the fitting curves are shown in Figure 4d. The correlation coefficients (R^2) of BC_R, BC_S, and BC_L obtained by Elovich model fitting were all greater than 0.91, indicating the great fitting effect. Therefore, we could infer that the adsorption process of heavy metal Cd^{2+} by BC_R, BC_S, and BC_L was not only the diffusion of the surface film but also the inhomogeneous diffusion of Cd^{2+} into the biochar to the multilayer adsorption [9]. The α was a constant positively related to the initial reaction rate, while β was a factor negatively correlated with the reaction rate, which was used to characterize the reaction activation capacity with the increase in the material surface coverage. Hence, compared with BC_R and BC_L, BC_S exhibited significantly higher α values and relatively low β, indicating its superior capability for rapid Cd^{2+} removal in water.

3.2.3. Study on Isothermal Equilibrium Cd^{2+} Adsorption by Biochar

The adsorption isotherm of biochar on Cd^{2+} was evaluated using the Langmuir and Freundlich models, with the fitting parameters presented in Tables 3 and 4. The data were well represented by both the Langmuir and Freundlich equations, yielding R^2 values ranging from 0.93 to 0.99. This suggests that the chemisorption of Cd^{2+} may take place on the uniform surfaces of the biochar. The K_L in the Langmuir model could imply the strength of adsorption capacity, and the constants n and K_F in the Freundlich model reflected the difficulty of adsorption. In addition, the binding energy of forming monolayer adsorption could also be reflected by K_L, so the reaction was recognized to be an endothermic reaction by the increased K_L with temperature. Due to the increasing K_L and K_F with the increase in temperature, $n > 0.5$, it was believed that the adsorption reaction of Cd^{2+} was easier with the increase in temperature. Since the Langmuir isotherm was a monolayer adsorption model, it can be inferred that the adsorption process of biochar to Cd^{2+} was dominated by chemical reactions.

Table 3. Langmuir fitting parameters of Cd^{2+} adsorption by BC_R, BC_S, and BC_L of *Iris sibirica* L.

	BC_R			**BC_S**			**BC_L**		
	K_L (L/mg)	**Q_{max} (mg/g)**	**R^2**	**K_L (L/mg)**	**Q_{max} (mg/g)**	**R^2**	**K_L (L/mg)**	**Q_{max} (mg/g)**	**R^2**
15 °C	0.018	1215.5	0.98	0.0089	1765.77	0.98	0.041	811.94	0.94
25 °C	0.14	759.71	0.96	0.034	1192.99	0.98	0.15	763.92	0.95
35 °C	0.23	713.65	0.94	0.086	832.45	0.96	0.24	723.17	0.93
45 °C	0.91	837.36	0.93	0.067	2606.11	0.94	0.92	840.98	0.93

Table 4. Freundlich fitting parameters of Cd^{2+} adsorption by BC_R, BC_S, and BC_L of *Iris sibirica* L.

	BC_R			**BC_S**			**BC_L**		
	K_F (mg/g)·(mg/L)$^{-n}$	**n**	**R^2**	**K_F (mg/g)·(mg/L)$^{-n}$**	**n**	**R^2**	**K_F (mg/g)·(mg/L)$^{-n}$**	**n**	**R^2**
15 °C	37.34	0.71	0.99	20.99	0.84	0.98	71.59	0.53	0.97
25 °C	115.27	0.57	0.98	50.9	0.75	0.98	126.07	0.54	0.98
35 °C	145.60	0.55	0.96	102.6	0.56	0.98	154.35	0.53	0.95
45 °C	380.74	0.55	0.95	171.63	0.84	0.95	383.50	0.55	0.95

Chi-square (χ^2) statistical analysis was introduced to complement R^2 values and provide a more comprehensive evaluation of the adsorption isotherm model fitting. The results demonstrated low χ^2 values, confirming the reliability of the Langmuir model (Table S2). A detailed comparison between theoretical adsorption capacities (q_x) and experimental values (q_{exp}) was conducted. The findings suggested that the predictions made by the Langmuir model aligned well with the data obtained from experiments. As shown in Table S3, the values of q_x closely matched q_{exp} values at higher initial Cd^{2+} concentrations, suggesting that the Langmuir model effectively described the monolayer adsorption behavior of Cd^{2+} onto BC_R, BC_S, and BC_L biochars. The Freundlich model parameter n was further discussed in terms of adsorption favorability. Although n values were slightly lower than 1, they still suggested moderately favorable adsorption conditions due to biochar surface heterogeneity (Table S4).

3.3. Research on the Mechanism of Biochar Adsorption to Cd^{2+}

3.3.1. The Influence of Elution Treatments on the Adsorption Effect

To study the impact and mechanism of biochar on the Cd^{2+} adsorption process, this research adopted different elution treatments to compare the adsorption capacity of biochar for Cd^{2+}. Firstly, water washing (group II) showed a substantial enhancement in the adsorption capacity of biochar for Cd^{2+}, indicating that the soluble ions were also removed after washing, reducing the competition of cations (K^+, Ca^{2+}, and Mg^{2+}) for Cd^{2+} adsorption. Moreover, it could also unblock the blocked pores on the surface of the biochar, thereby providing more adsorption sites. As depicted in Figure 5a, the adsorption of Cd^{2+} in groups II and IV was almost the same, indicating that the target pollutant Cd^{2+} could be removed by precipitation after increasing the pH, so the process of precipitation was significant in the elimination of Cd^{2+}. However, the adsorption of Cd^{2+} on the biochar decreased significantly after pickling (group III) by 71.93%, 75.06%, and 63.96%, respectively, which could be ascribed to the removal of inorganic minerals on the surface of the biochar and reduced pH after pickling. Relevant studies found that H^+ ions will react with the anions, such as HCO^{3-}, $CO_3{}^{2-}$, and $SO_4{}^{2-}$, in biochar, reducing the alkalinity of biochar solution, thereby weakening the precipitation effect of biochar [46]. Consequently, enhancing the pH levels could greatly increase biochar's ability to adsorb Cd^{2+}. Metal ions (including K^+, Ca^{2+}, and Mg^{2+}) were captured in biochar via direct electrostatic interaction and the creation of complexes with carboxyl and hydroxyl functional groups. In the adsorption process, these metals may be replaced by Cd^{2+} present in the solution as a result of electrostatic cation exchange, reactions involving metal exchange of surface complexes, and co-precipitation. Therefore, metal ion exchange as a common mechanism for the adsorption of Cd^{2+} by biochar could not be ignored. To further illustrate the effect of ion exchange, we compared the changes in common metal concentrations in the solution after biochar adsorption of Cd^{2+} under different elution treatment conditions, as shown in Figure 5b–d. Under different elution conditions, the K^+, Ca^{2+}, and Mg^{2+} in the solution increased after biochar adsorbed Cd^{2+} by ion exchange. In addition, the change in the ion concentration after acid washing of biochar was significantly reduced (group III), which was consistent with its weakened adsorption capacity, indicating that ion exchange was one of the main contributions of adsorption. Regardless of the treatment conditions, the amount of K^+ within the solution following Cd^{2+} adsorption by biochar changed most observably, so it could be inferred that K^+ was the easiest to ion exchange with Cd^{2+}.

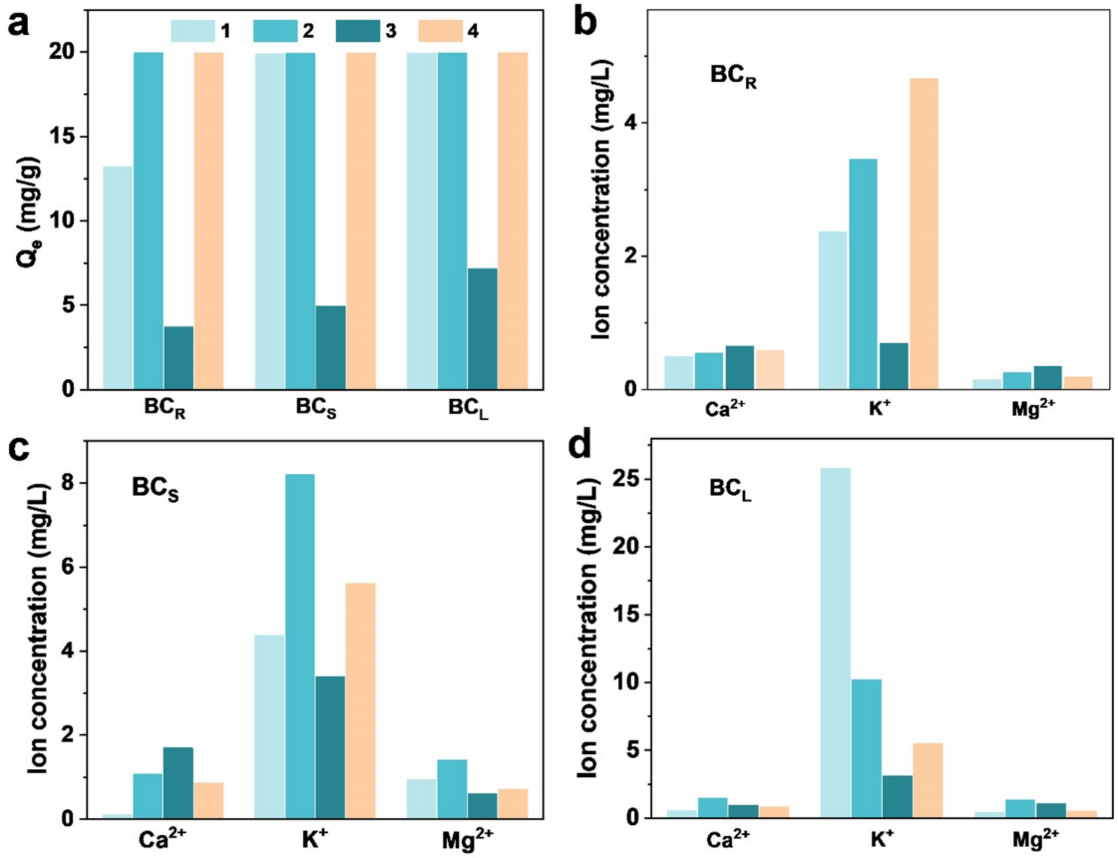

Figure 5. (**a**) Adsorption effect of Cd^{2+} by biochar with different elution treatments. Changes of common metal concentration in solution after biochar adsorbs Cd^{2+} under different elution treatment conditions: (**b**) BC_R, (**c**) BC_S, and (**d**) BC_L. Group I was untreated biochar, group II was biochar after washing and drying, group III was biochar after acid washing and drying, and group IV was biochar after acid washing and adjusting the pH to the original pH (time 5–1440 min, initial Cd^{2+} concentration 20.00 mg/L, $NaNO_3$ concentration 0.01 mol/L, temperature 25 °C, volume 20.00 mL, and dosage of biochar 0.02 g).

3.3.2. Contribution of Cd^{2+} Adsorption Mechanism

During the adsorption procedure of biochar for Cd^{2+}, the adsorption mechanism could be divided into precipitation, ion exchange, and others (surface complexation and coordination of Cd^{2+} with π electrons). Based on the adsorption characteristics of Cd^{2+} on both the original biochar and various elution biochars, the various processes contributing to the adsorption of Cd^{2+} were assessed using the method outlined in the Section 2, as shown in Figure 6. Obviously, ion exchange accounted for the main contribution to the Cd^{2+} adsorption process, reaching to 32%, 54%, and 65% of BC_R, BC_S, and BC_L, respectively. In addition, the contribution of precipitation in Cd^{2+} adsorption cannot be ignored, especially in BC_R accounting for 46%, thus it was advantageous for the treatment of acidic wastewater. Other mechanisms of Cd^{2+} adsorption did not account for a large contribution, including surface complexation and coordination of Cd^{2+} with π electrons. Therefore, BC_R was a suitable choice for the treatment of acidic soils due to the dominant precipitation, BC_S was appropriate for the treatment of Cd-containing wastewater by its maximum adsorption capacity, and BC_L could be used as a potash fertilizer additive based on high K^+ leaching.

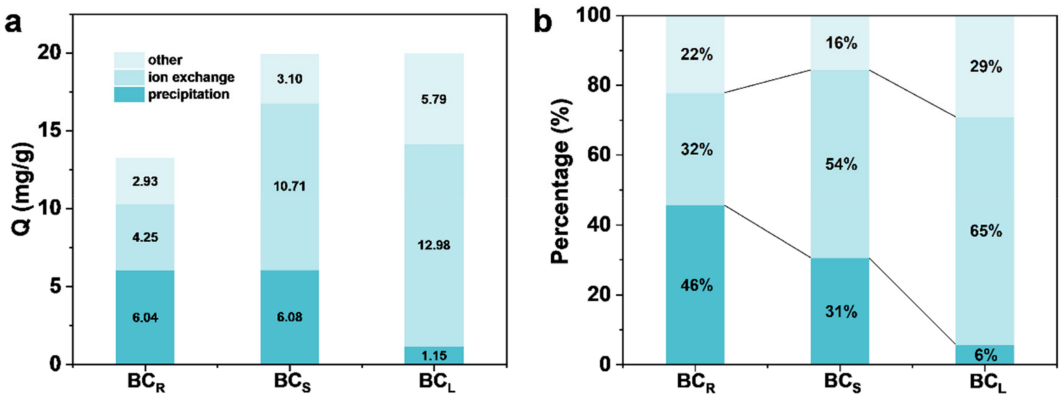

Figure 6. (**a**) The contribution to Cd^{2+} adsorption by metal ion exchange (Q_{cme}), precipitation with minerals (Q_{cmp}), and others (M_{other}) on biochars. (**b**) The proportion of contribution from various mechanisms to Cd^{2+} adsorption on BC_R, BC_S, and BC_L (time 5–1440 min, initial Cd^{2+} concentration 20.00 mg/L, volume 20.00 mL, $NaNO_3$ concentration 0.01 mol/L, temperature 25 °C, dosage of biochar 0.02 g, and pH 5.5).

3.4. Evaluation

The adsorptive behavior of Cd^{2+} on biochar was systematically analyzed. The BC_S was more beneficial for the fast elimination of Cd^{2+} via superior α and relatively low β in the Elovich model and obtained the best adsorption efficiency by contrasting the peak adsorption capability (2606.11 mg/g) based on the Langmuir model. The adsorption capacity could be significantly affected by acid washing or pH adjustment, which indicated that precipitation was an important mechanism of Cd^{2+} adsorption. H^+ ions would react with the anions, such as HCO_3^-, CO_3^{2-}, and SO_4^{2-}, in biochar, reducing the alkalinity of biochar solution, thereby weakening the precipitation effect of biochar. By comparing the changes in ion concentration after adsorption, it can be seen that ion exchange was also the main contribution of adsorption. Numerous metal ions, including K^+, Ca^{2+}, and Mg^{2+}, were retained in biochar through direct electrostatic attraction and by forming complexes with carboxyl and hydroxyl functional groups. In the solution, these metals are capable of being replaced by Cd^{2+} due to processes such as static electrical cation exchange, metal substitution reactions through surface complexes, and concurrent precipitation, which occur during the adsorption process; among them, K^+ is the most readily exchanged with Cd^{2+}. Therefore, the adsorption mechanism can be categorized into precipitation, ion exchange, and other mechanisms (surface complexation and coordination of Cd^{2+} with π electrons). Among them, due to the more complex pore structure and abundant micropore volume, the proportion of ion exchange significantly increased in BC_S and BC_L, reaching 54% and 65%, respectively, compared to 32% in BC_R, resulting in higher adsorption capacities for Cd^{2+}. In addition, the contribution of precipitation to Cd^{2+} adsorption in BC_R accounted for 46%, thus it was advantageous for the treatment of acidic wastewater, whereas the BC_S and BC_L were suitable for neutral or alkaline adsorption environments. Specially, BC_L with a high potassium content could also be used as potash fertilizer.

3.5. Investigation of Desorption and Recycling Process

To assess the viability and expandability of the biochar, it was essential to examine its ability to desorb and be reused. This investigation involved conducting desorption experiments on the BC_S, which demonstrated the highest sorption efficiency. The assessment of BC_S' recyclability was carried out over five successive adsorption–desorption cycles. Before initiating each cycle, the sorbent was washed with deionized water. As illustrated in Figure 7, the results showed that the sorbent retained its stability throughout the five cycles, even though there was a slight reduction in sorption efficiency, decreasing from 99.45% to

87.96%. The minor decrease in performance was due to the slight structural deterioration of the biochar and possible obstruction of some active sites by residual Cd^{2+} ions [42].

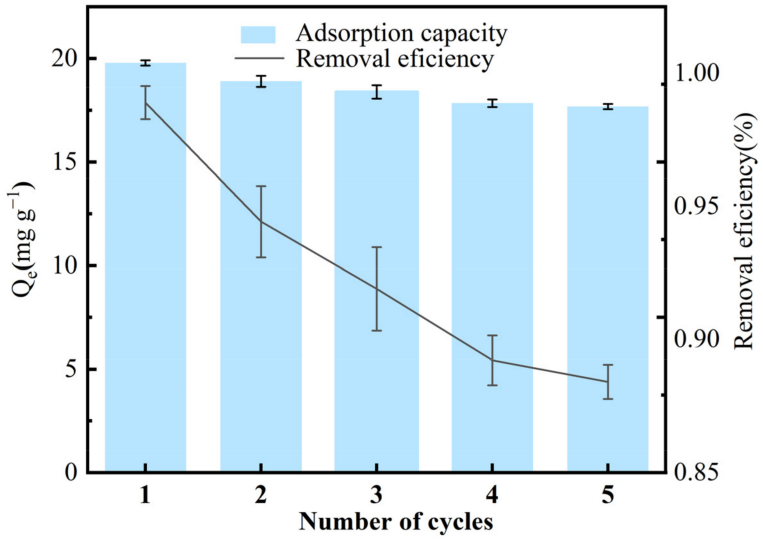

Figure 7. Effect of adsorption–desorption cycles on adsorption capacities and removal efficiency of Cd^{2+} by BC_S.

4. Conclusions

This study demonstrated the feasibility of different parts of *Iris sibirica* L. to synthesize BC_R, BC_S, and BC_L and explored the basic properties and effects of removing Cd^{2+} in wastewater. Experiments conducted for adsorption analysis showed that BC_R, BC_S, and BC_L showed a significant adsorption capacity for Cd^{2+}, with maximum uptake amounts reaching 13.22, 19.92, and 19.89 mg/g. Particularly, BC_S possessed a significant pore structure featuring a high SSA, along with diverse kinds of surface functional groups, including carboxyl groups, phenolic hydroxyl groups, and acid anhydrides, as characterized by SEM and FTIR analyses. Based on the analysis of adsorption fitting, the adsorption mechanism on as-prepared biochar might be totally governed by the chemical adsorption process, including transfer and movement of electrons between the adsorbent and Cd^{2+}. Additionally, the mechanisms of ion exchange were more superior in BC_L and BC_S compared with BC_R. In contrast, the precipitation mechanism was the primary factor in the adsorption process of Cd^{2+} by BC_R. Therefore, BC_R was recognized as a better choice for the acidic wastewater treatment. Moreover, the adsorbents obtained from *Iris sibirica* L. are inexpensive by-products, thus offering a sustainable and scalable approach for the treatment of industrial wastewater. Additionally, the enduring effectiveness of biochars highlighted their ability to maintain adsorption efficiency with minimal material degradation, reducing the need for regular replacements. This not only improves their scalability but also bolsters the economic feasibility of large-scale operations in wastewater treatment.

Supplementary Materials: The following supporting information can be downloaded at: https://www.mdpi.com/article/10.3390/pr13051520/s1, Table S1: Comparison of the adsorption capacity of BCR, BCS and BCL with the other adsorbent in the Literature. Table S2: Chi-square (χ2) test results of Langmuir fitting for Cd2+ adsorption by BCR, BCS and BCL at different temperatures. Table S3: Chi-square (χ2) test results of Langmuir fitting for Cd2+ adsorption by BCR, BCS and BCL at different temperatures. Table S4: Freundlich isotherm parameters (KF, n) of Cd2+ adsorption by BCR, BCS and BCL at different temperatures.

Author Contributions: Conceptualization, T.L. and L.W.; Methodology, Y.W. and Y.N.; Validation, Y.W. and Y.N.; Formal analysis, T.L., Z.Z. and J.L. (Jin Liu); Investigation, Y.W., Y.N., Z.Z. and J.L. (Jin

Liu); Writing–review & editing, Y.W., Y.N., X.W., J.W., J.L. (Ji Li) and L.W.; Supervision, X.W. and L.W.; Funding acquisition, T.L. and L.W. All authors have read and agreed to the published version of the manuscript.

Funding: This study was supported by the Guangdong Basic and Applied Basic Research Foundation (2024A1515030123), the Shenzhen Science and Technology Innovation Commission (20231128105823001), and the Shenzhen Polytechnic Scientific Research Initiation Project (6023310038K, 6024271015K).

Data Availability Statement: The original contributions presented in this study are included in the article/Supplementary Materials. Further inquiries can be directed to the corresponding author.

Conflicts of Interest: Author Yongchao Niu was employed by the Bceg Environmental Remediation Co., Ltd.; author Zhonglei Zhang was employed by China North Energy Conservation and Environment Protection Co., Ltd. The remaining authors declare that the research was conducted in the absence of any commercial or financial relationships that could be construed as a potential conflict of interest.

References

1. Clabeaux, B.L.; Navarro, D.A.; Aga, D.S.; Bisson, M.A. Combined effects of cadmium and zinc on growth, tolerance, and metal accumulation in Chara australis and enhanced phytoextraction using EDTA. *Ecotoxicol. Environ. Saf.* **2013**, *98*, 236–243. [CrossRef]
2. Chen, Q.Y.; DesMarais, T.; Costa, M. Metals and mechanisms of carcinogenesis. *Annu. Rev. Pharmacool. Toxicol.* **2019**, *59*, 537–554. [CrossRef]
3. Liu, S.; Ali, S.; Yang, R.; Tao, J.; Ren, B. A newly discovered Cd-hyperaccumulator *Lantana camara* L. *J. Hazard. Mater.* **2019**, *371*, 233–242. [CrossRef]
4. Zhu, Y.; Wang, H.; Lv, X.; Zhang, Y.; Wang, W. Effects of biochar and biofertilizer on cadmium-contaminated cotton growth and the antioxidative defense system. *Sci. Rep.* **2020**, *10*, 20112. [CrossRef]
5. Liu, C.; Guo, B.; Li, H.; Fu, Q.; Li, N.; Lin, Y.; Xu, G. Azolla incorporation under flooding reduces grain cadmium accumulation by decreasing soil redox potential. *Sci. Rep.* **2021**, *11*, 6325. [CrossRef]
6. Liu, X.; Yin, L.; Deng, X.; Gong, D.; Du, S.; Wang, S.; Zhang, Z. Combined application of silicon and nitric oxide jointly alleviated cadmium accumulation and toxicity in maize. *J. Hazard. Mater.* **2020**, *395*, 122679. [CrossRef]
7. Yap, M.W.; Mubarak, N.M.; Sahu, J.N.; Abdullah, E.C. Microwave induced synthesis of magnetic biochar from agricultural biomass for removal of lead and cadmium from wastewater. *J. Ind. Eng. Chem.* **2017**, *45*, 287–295. [CrossRef]
8. Park, J.-H.; Ok, Y.S.; Kim, S.-H.; Cho, J.-S.; Heo, J.-S.; Delaune, R.D.; Seo, D.-C. Competitive adsorption of heavy metals onto sesame straw biochar in aqueous solutions. *Chemosphere* **2016**, *142*, 77–83. [CrossRef]
9. Sebastian, A.; Nangia, A.; Prasad, M. Cadmium and sodium adsorption properties of magnetite nanoparticles synthesized from *Hevea brasiliensis* Muell. Arg. bark: Relevance in amelioration of metal stress in rice. *J. Hazard. Mater.* **2019**, *371*, 261–272. [CrossRef]
10. Tan, X.-F.; Liu, Y.-G.; Gu, Y.-L.; Xu, Y.; Zeng, G.-M.; Hu, X.-J.; Liu, S.-B.; Wang, X.; Liu, S.-M.; Li, J. Biochar-based nano-composites for the decontamination of wastewater: A review. *Bioresour. Technol.* **2016**, *212*, 318–333. [CrossRef]
11. Rutigliano, F.A.; Romano, M.; Marzaioli, R.; Baglivo, I.; Baronti, S.; Miglietta, F.; Castaldi, S. Effect of biochar addition on soil microbial community in a wheat crop. *Eur. J. Soil Biol.* **2014**, *60*, 9–15. [CrossRef]
12. Wang, S.S.; Gao, B.; Zimmerman, A.R.; Li, Y.C.; Ma, L.N.; Harris, W.G.; Migliaccio, K.W. Physicochemical and sorptive properties of biochars derived from woody and herbaceous biomass. *Chemosphere* **2015**, *134*, 257–262. [CrossRef]
13. Ahmad, M.; Lee, S.S.; Dou, X.; Mohan, D.; Sung, J.-K.; Yang, J.E.; Ok, Y.S. Effects of pyrolysis temperature on soybean stover- and peanut shell-derived biochar properties and TCE adsorption in water. *Bioresour. Technol.* **2012**, *118*, 536–544. [CrossRef]
14. Lo, S.-F.; Wang, S.-Y.; Tsai, M.-J.; Lin, L.-D. Adsorption capacity and removal efficiency of heavy metal ions by Moso and Ma bamboo activated carbons. *Chem. Eng. Res. Des.* **2012**, *90*, 1397–1406. [CrossRef]
15. Li, Z.; Qi, X.; Fan, X.; Du, Z.; Hu, C.; Zhao, Z.; Isa, Y.; Liu, Y. Amending the seedling bed of eggplant with biochar can further immobilize Cd in contaminated soils. *Sci. Total Environ.* **2016**, *572*, 626–633. [CrossRef]
16. Cheng, Q.; Huang, Q.; Khan, S.; Liu, Y.; Liao, Z.; Li, G.; Ok, Y.S. Adsorption of Cd by peanut husks and peanut husk biochar from aqueous solutions. *Ecol. Eng.* **2016**, *87*, 240–245. [CrossRef]
17. Cui, X.Q.; Fang, S.Y.; Yao, Y.Q.; Li, T.Q.; Ni, Q.J.; Yang, X.E.; He, Z.L. Potential mechanisms of cadmium removal from aqueous solution by Canna indica derived biochar. *Sci. Total Environ.* **2016**, *562*, 517–525. [CrossRef]

18. Kim, W.-K.; Shim, T.; Kim, Y.-S.; Hyun, S.; Ryu, C.; Park, Y.-K.; Jung, J. Characterization of cadmium removal from aqueous solution by biochar produced from a giant Miscanthus at different pyrolytic temperatures. *Bioresour. Technol.* **2013**, *138*, 266–270. [CrossRef]
19. Ahmad, M.; Rajapaksha, A.U.; Lim, J.E.; Zhang, M.; Bolan, N.; Mohan, D.; Vithanage, M.; Lee, S.S.; Ok, Y.S. Biochar as a sorbent for contaminant management in soil and water: A review. *Chemosphere* **2014**, *99*, 19–33. [CrossRef]
20. Sun, J.; Lian, F.; Liu, Z.; Zhu, L.; Song, Z. Biochars derived from various crop straws: Characterization and Cd (II) removal potential. *Ecotoxicol. Environ. Saf.* **2014**, *106*, 226–231. [CrossRef]
21. Cao, X.; Ma, L.; Gao, B.; Harris, W. Dairy-manure derived biochar effectively sorbs lead and atrazine. *Environ. Sci. Technol.* **2009**, *43*, 3285–3291. [CrossRef]
22. Sewu, D.D.; Boakye, P.; Woo, S.H. Highly efficient adsorption of cationic dye by biochar produced with Korean cabbage waste. *Bioresour. Technol.* **2017**, *224*, 206–213. [CrossRef]
23. Wang, Z.; Liu, G.; Zheng, H.; Li, F.; Ngo, H.H.; Guo, W.; Liu, C.; Chen, L.; Xing, B. Investigating the mechanisms of biochar's removal of lead from solution. *Bioresour. Technol.* **2015**, *177*, 308–317. [CrossRef]
24. Jia, Y.H.; Shi, S.L.; Liu, J.; Su, S.M.; Liang, Q.; Zeng, X.B.; Li, T.S. Study of the Effect of Pyrolysis Temperature on the Cd^{2+} Adsorption Characteristics of Biochar. *Appl. Sci.* **2018**, *8*, 1019. [CrossRef]
25. Zhang, L.M.; Ren, Y.F.; Xue, Y.H.; Cui, Z.W.; Wei, Q.H.; Han, C.; He, J.Y. Preparation of biochar by mango peel and its adsorption characteristics of Cd(ii) in solution. *Rsc Adv.* **2020**, *10*, 35878–35888. [CrossRef]
26. Morgan, H.M., Jr.; Jiang, T.J.; Tsai, W.T.; Yen, T.B. Initial physiochemical characterization of Djulis (*Chenopodium formosanum*) spent mushroom substrate biochar and its application for methylene blue dye adsorption, isotherm, kinetics, and parameters. *Biomass Convers. Biorefinery* **2025**, 1–15. [CrossRef]
27. Nguyen, D.T.; Hoang, T.K.; Tran, T.D.; Nguyen, M.H.; Trinh, K.T.; Khuong, D.A.; Tsubota, T.; Pham, T.D. Adsorption characteristics of individual and binary mixture of ciprofloxacin antibiotic and lead(II) on synthesized bamboo-biochar. *Environ. Res.* **2025**, *273*, 121225. [CrossRef]
28. *ASTM D1782-84*; Standard Practice for Operating Salt Spray (Fog) Apparatus. ASTM International: West Conshohocken, PA, USA, 1984.
29. Cao, X.; Zhong, L.; Peng, X.; Sun, S.; Li, S.; Liu, S.; Sun, R. Comparative study of the pyrolysis of lignocellulose and its major components: Characterization and overall distribution of their biochars and volatiles. *Bioresour. Technol.* **2014**, *155*, 21–27. [CrossRef]
30. Yuan, J.-H.; Xu, R.-K.; Zhang, H. The forms of alkalis in the biochar produced from crop residues at different temperatures. *Bioresour. Technol.* **2011**, *102*, 3488–3497. [CrossRef]
31. Kamari, S.; Shahbazi, A. Biocompatible Fe_3O_4@SiO_2-NH_2 nanocomposite as a green nanofiller embedded in PES–nanofiltration membrane matrix for salts, heavy metal ion and dye removal: Long–term operation and reusability tests. *Chemosphere* **2020**, *243*, 125282. [CrossRef]
32. Downie, A.; Crosky, A.; Munroe, P. Physical properties of biochar. In *Biochar for Environmental Management*; Routledge: London, UK, 2012; pp. 45–64. [CrossRef]
33. Wu, W.; Yang, M.; Feng, Q.; McGrouther, K.; Wang, H.; Lu, H.; Chen, Y. Chemical characterization of rice straw-derived biochar for soil amendment. *Biomass Bioenergy* **2012**, *47*, 268–276. [CrossRef]
34. Cantrell, K.B.; Hunt, P.G.; Uchimiya, M.; Novak, J.M.; Ro, K.S. Impact of pyrolysis temperature and manure source on physicochemical characteristics of biochar. *Bioresour. Technol.* **2012**, *107*, 419–428. [CrossRef] [PubMed]
35. Stefanovsky, S.V.; Stefanovsky, O.I.; Prusakov, I.L.; Kadyko, M.I.; Averin, A.A.; Nikonov, B.S. Speciation of sulphate ions in sodium alumino(iron)phosphate glasses. *J. Non-Cryst. Solids* **2019**, *512*, 81–89. [CrossRef]
36. Yasushi Suetsugu, I.S.; Tanaka, J. Configuration of Carbonate Ions in Apatite Structure Determined by Polarized Infrared Spectroscopy. *J. Am. Ceram. Soc.* **1998**, *81*, 746–748. [CrossRef]
37. Fonseca, J.D.D.; Matej-Lukowicz, K.; Kluska, J.; Baluk, M.A.; Kulesza, J.; Barros, B.S.; Wojciechowska, E. Effect of synthesis method on ammonium sorption behavior of oat husk biochar. *Sci. Rep.* **2025**, *15*, 11143. [CrossRef]
38. Marsolla, L.D.; Brito, G.M.; Freitas, J.C.C.; Cabral Coelho, E.R. Sustainable enhancement of biochar and biochar composite properties through temperature-controlled pyrolysis of agricultural biomass and marble waste. *Waste Manag.* **2025**, *201*, 114799. [CrossRef]
39. Mahmoodi, N.M.; Oveisi, M.; Taghizadeh, A.; Taghizadeh, M. Synthesis of pearl necklace-like ZIF-8@chitosan/PVA nanofiber with synergistic effect for recycling aqueous dye removal. *Carbohydr. Polym.* **2020**, *227*, 115364. [CrossRef]
40. Wang, X.; Liu, N.; Liu, Y.; Jiang, L.; Zeng, G.; Tan, X.; Liu, S.; Yin, Z.; Tian, S.; Li, J. Adsorption removal of 17β-estradiol from water by rice straw-derived biochar with special attention to pyrolysis temperature and background chemistry. *Int. J. Environ. Res. Public Health* **2017**, *14*, 1213. [CrossRef]

41. Zeng, Z.-w.; Tan, X.-f.; Liu, Y.-g.; Tian, S.-r.; Zeng, G.-m.; Jiang, L.-h.; Liu, S.-b.; Li, J.; Liu, N.; Yin, Z.-h. Comprehensive adsorption studies of doxycycline and ciprofloxacin antibiotics by biochars prepared at different temperatures. *Front. Chem.* **2018**, *6*, 80. [CrossRef]
42. Arora, B.; Dhillayan, D.; Yadav, S.; Ghotekar, S.; Mukherjee, S.; Mohan, C.; Kataria, N. Bio-fabrication of acid-treated and magnetic biochar from rice straw for tetracycline removal from water: Response surface methodology study, reusability, and modelling. *Biomass Convers. Biorefinery* **2025**, 1–16. [CrossRef]
43. Gado, W.S.; Morshedy, A.S.; Entsar; Taha, H.; El-Zahhar, A.A.; Alghamdi, M.M.; El Naggar, A.M.A.; El-Fawal, E.M. Efficient removal of cadmium ions from wastewater using metal oxide-doped sunflower stem-generated biochar: Sorption mechanism and performance. *Biomass Convers. Biorefinery* **2025**, 1–24. [CrossRef]
44. Xiang, A.H.; Gao, Z.N.; Zhang, K.; Jiang, E.C.; Ren, Y.Z.; Wang, M.F. Study on the Cd (II) adsorption of biochar based carbon fertilizer. *Ind. Crops Prod.* **2021**, *174*, 114213. [CrossRef]
45. Yao, Y.; Gao, B.; Inyang, M.; Zimmerman, A.R.; Cao, X.; Pullammanappallil, P.; Yang, L. Biochar derived from anaerobically digested sugar beet tailings: Characterization and phosphate removal potential. *Bioresour. Technol.* **2011**, *102*, 6273–6278. [CrossRef] [PubMed]
46. Sabermahani, F.; Taher, M.A. Polyacrylic acid-modified alumina for solid-phase extraction and preconcentration of trace iron and chromium from plant samples. *J. AOAC Int.* **2011**, *94*, 1918–1924. [CrossRef]

Disclaimer/Publisher's Note: The statements, opinions and data contained in all publications are solely those of the individual author(s) and contributor(s) and not of MDPI and/or the editor(s). MDPI and/or the editor(s) disclaim responsibility for any injury to people or property resulting from any ideas, methods, instructions or products referred to in the content.